

EAD and Pulse Circulation in a 1D Ring –Shaped Cardiac Tissue with Pronounced Effect of Ca^{2+} Dynamics.

(Computer Simulation Study)

B. Kogan, R. Huffaker, S. Lamp, J. Weiss.

Abstract

Pulse propagation in a ring of cardiac tissue is a subject of significant practical and theoretical importance, particularly in understanding the mechanisms of many life-threatening cardiac tachyarrhythmias. Most of the previous theoretical and computer simulation studies were performed without taking into consideration the major properties of intracellular Ca^{2+} dynamics. These studies showed that the steady state, unstable (quasi-periodic), and terminating regimes of propagation could exist depending on ring length. Unstable propagation required the action potential duration (APD) restitution curve to have slope $\gamma \geq 1$ for some region of diastolic interval (DI).

Our recent simulation studies with a ring composed of Luo and Rudy cell models with modified $[\text{Ca}^{2+}]_i$ dynamics showed that (for some ring length) unstable irregular propagation replaced the quasi-periodic and occurred even when $\gamma < 1$ over all ranges of DI. The mechanism supporting irregular propagation in this case is not clear.

Based on the presented simulation results, the mechanism of irregular propagation can be formulated as follows. Shortening of the ring length causes the pacing rate of each cell in the ring to increase, leading after some time to intracellular Ca accumulation and subsequent spontaneous Ca^{2+} release from sarcoplasmic reticulum (SR). These processes affect Ca-sensitive membrane currents, changing the shape of the action potential and increasing APD and its uneven distribution along the ring cells. The increase of APD is accompanied by a corresponding increase of propagated wavelength. For short rings, the propagation phenomena are different when reaction of Ca-sensitive membrane currents is normal versus when it is amplified, e.g. by decreasing the coefficient $K_{\text{mns}(\text{Ca})}$.

In the first case, after the end of initial transient period, the growth of the wavelength in time (after a few turns of circulation) causes the alternance of the major wave propagation characteristics. This is followed by a bump on and breakup of the wave tail, and sharp decrease of propagation velocity when front of the wave approaches its tail. Regeneration of the propagated wave occurs due to the effect of local currents, but only after the cells at the tail have gone out of excitation.

In the second case, regeneration occurs after a temporary stop of the wave due to the appearance of cells with early after depolarization (EAD) in some region of the ring. In this case, two wave fronts may be observed moving in the same or opposite directions. EAD results from distortion of the balance of cell repolarization currents, leading to a prevailing total inward current.

Introduction

Pulse propagation in a ring of cardiac tissue is a subject of significant practical and theoretical importance [1-3]. In particular, the study of this phenomenon facilitates an

understanding of the mechanisms of many life-threatening cardiac tachyarrhythmias. The physiological studies of pulse propagation in a ring-shaped preparation of certain length of atrial tissue [4, 5] show irregular oscillations of action potential duration (APD), period of circulation, and conduction velocity (CV). Most of the previous theoretical and computer simulation studies [6,7, 8, 9] of propagation phenomena in tissue of such configuration did not consider the effect of intracellular Ca^{2+} dynamics. Depending on the ring length changing (in decreasing order), these investigations demonstrate the steady state, unstable, and terminating regimes of propagation. It was also shown that unstable propagation requires the APD restitution curve (measured in cell inside a tissue) should have a slope $\gamma \geq 1$ for some region of DI. The DI for which $\gamma = 1$ determines the critical value of ring length when unstable propagation begins through infinite-dimensional Hopf bifurcation [7, 8].

At the same time, the study with intracellular Ca^{2+} dynamics [10] shows that unstable irregular propagation can be observed for some ring length even when $\gamma < 1$ for all range of DI. Intracellular Ca^{2+} dynamics play a major role in the process of excitation-contraction coupling and also produce a feedback effect changing the shape and increasing duration of AP through Ca-sensitive ionic currents (Ca-activated nonselective current, L-type Ca channel current, Ca-activated Cl current and NA-Ca exchange current). This feedback effect significantly increases with increase of cell pacing rate due to intracellular $[\text{Ca}]_i$ accumulation and subsequent spontaneous Ca^{2+} release from sarcoplasmic reticulum (SR). Ca^{2+} accumulation and SR spontaneous release, as well as EADs were observed in physiological experiments with single cardiac cell [11, 12]

When excitation wave propagates in a ring – shaped tissue, each cell in the tissue is paced by local current with rate inversely proportional to the period of circulation or to the ring length. Thus, by progressive shortening the ring length it is possible to find one when after several turns of pulse circulation the front of the wave will turn out to be close to its tail and velocity of wave propagation significantly falls. This occurs due to increased APD and corresponding wavelength under increased effect of Ca^{2+} dynamics during high pacing rate. Moreover, it is possible to observe bumps on a wave tail, which indicate the nonmonotonous distribution of APD along the ring cells going out of excitation (see [10]). As cells of the tail begin to fully repolarize, the velocity of the front regenerates.

Additionally, when the sensitivity to $[\text{Ca}^{2+}]_i$ of certain Ca-dependent membrane currents is increased (e.g. decreasing the coefficient $K_{\text{mns}(\text{Ca})}$ from typical value 1.2 mM to 0.9 mM), the regeneration of wave propagation occurs due to the appearance of EADs in some region of the wave tail. In some cases two wave fronts appear, moving in the same or opposite direction.

The mechanism of the wave propagation regeneration is not clear. We hypothesize that the effect of Ca^{2+} dynamics (under condition of high pacing rate) expressed in the increasing of APD up to appearance of EADs is responsible for regeneration of wave propagation. To prove this hypothesis we have undertaken a series of computer simulation experiments amplifying the effect of Ca^{2+} dynamics in tissue cells by increasing the sensitivity of $I_{\text{ns}(\text{Ca})}$ to $[\text{Ca}^{2+}]_i$ (decreasing coefficient $K_{\text{mns}(\text{Ca})}$). In this paper we present the obtained results and its explanation.

METHODS

The mathematical model of wave propagation in 1D tissue is described by the following partial differential equation:

$$\frac{\partial V}{\partial t} = D \frac{\partial^2 V}{\partial x^2} + (I_m + I_{st}(s, t)) \frac{1}{C_m} \quad (1)$$

with appropriate initial and boundary conditions.

Here V is membrane potential, D is a diffusion coefficient, I_{st} is the external stimulating current, and C_m is a membrane capacity. To make the above equation closed, it is necessary to add the system of nonlinear ordinary differential equations (ODEs) that describes the behavior of all components of I_m and processes in intracellular compartments. For this purpose we have chosen the AP model proposed in [13], which represents a modification of the Luo-Rudy AP model [14]. The initial conditions were chosen the same as in [13], except with slight modifications to $[Ca^{2+}]_{i,tot}$ (from 18.61 to 21.01 μM) and $[Ca^{2+}]_{j,sr,tot}$ (from 8.44 to 6.9 mM).

For computer simulation, a ring is formed from the original line of equidistant cell models (nodes) interconnected by diffusion. After stimulation of one end of this line and formation of the propagated wave of full length, the line is closed numerically into a ring. To change the ring length, the same procedure is repeated but with different number of nodes.

Computer simulations were performed on IBM SP massively parallel computer using the splitting operator algorithm [15]. According to this algorithm the integration (1)

is split into two parts: integration of diffusion equation $\frac{\partial V}{\partial t} = D \frac{\partial^2 V}{\partial x^2}$, and integration of the system of ODEs $\frac{\partial V}{\partial t} = (I_m + I_{st}) \frac{1}{C_m}$. These integrations are executed in consecutive

time cycles of predetermined duration Δt . The specific features of this algorithm are described in [16,17]. The splitting operator algorithm allows integration of the system of nonlinear ODEs at any point in space independently and with variable time steps. In all computer simulations, the time step Δt for ODE solutions varied from 0.005-0.1 ms and the space step Δx was fixed at 0.016 cm. These choices provide stability and accuracy with the chosen numerical integration method, and do not disturb the conditions of medium continuity (see [18]). Specifically, an explicit Euler numerical method was used

to solve the diffusion equation, for which the stability condition is $\Delta t \leq \frac{\Delta x^2}{2D}$. For

$\Delta x = 0.016$ cm and $D = 1$ cm²/s, the critical value is $\Delta t = 0.128$ ms. In our computations this equation is solved twice in one computational cycle, with $\Delta t = 0.05$ ms. The problem of computational error arises for solutions to the system of nonlinear ODEs describing the fast membrane processes during depolarization phase of the AP. To decrease these errors, we use the Euler explicit method with variable time steps, which are changed depending on the rate of the most rapid variable. In addition, for fast sodium channel gate variable, we replace the Euler method with the so-called hybrid method [19].

The continuity condition proposed by Winfree [18] requires that the chosen space step Δx satisfies the inequality $D > \Delta x^2 / T_r$. Here T_r is an activation rising time measured in a cell placed in tissue. This time is longer than in an isolated cell due to the effect of the local currents and incomplete recovery of cell I_{Na} during wave circulation in a comparatively short ring length. Estimating $T_r = 2.5$ ms, we finding that by $D = 1$ cm²/s and $\Delta x = 0.016$ cm this inequality is well satisfied.

Individual nodes are distinguished by their position in the initial line of cells before it is closed. Node i is defined as the i^{th} node in the line, for $0 \leq i \leq N-1$, where N is total number of nodes in the ring. The position of node i in the closed ring (in cm), after k turns of the circulating wave, is defined as $(k-1)*L + i*\Delta x$, where L is the length of the ring in cm.

APD is calculated for each AP of each node in the ring and graphed as a function of the position in the ring. For long rings, APD is calculated using AP₉₀ level. For shorter rings, when propagation is less regular, APD is calculated on a level of -50 mV. The error associated with this calculation is approximately 2 ms, the amount of time required for a potential change of 1 mV in a cell near the tail of an elongated wave.

Velocity of wave propagation is calculated as a function of position in the ring. The formula for velocity defines the front of the wave at time T_i as the node X_i where the maximum value of $V_i - V_{i+1}$ occurs. The velocity is found by measuring the average of the time elapsed while the wave propagated from node X_{i-k} to node X_i and the time elapsed while the wave propagated from node X_i to node X_{i+k} , for some suitably chosen k . The formula is:

$$U_i = \frac{1}{2} \left(\frac{X_i - X_{i-k}}{T_i - T_{i-k}} + \frac{X_{i+k} - X_i}{T_{i+k} - T_i} \right)$$

The error from this formula, defining θ as the real conduction velocity, is given by the formula [19]:

$$\frac{\theta}{1 + \frac{\theta}{2kS}} \leq U \leq \frac{\theta}{1 - \frac{\theta}{2kS}}$$

Here S is defined as the quotient of the space step ΔX and the time step ΔT . In our simulation, ΔX is 0.016 cm, ΔT is 0.1 ms, and k is 5, giving a maximum error of $|U - \theta| < 3.2$ cm/s.

Results

a. Stationary propagation in a rings of long length with different $K_{mns(Ca)}$

Ring of 51.2 cm (3200 nodes) yields a pacing rate about one per $T=960$ ms, which corresponds roughly to normal pacing rate in a human heart. In this case (see Fig.1 A, B) the stationary propagation is established for both $K_{mnc(Ca)} = 1.2$ mM and 0.9 mM. The APD and velocity of propagation, θ , are fairly constant over five turns of wave circulation in both cases. The amplitude and time characteristics of AP and $[Ca^{2+}]_i$ are not changed because under this rate of stimulation the Ca accumulation and its following spontaneous release from SR do not occur.

b. Irregular propagation

The beginning of irregular propagation is observed in the distribution in space of APD and velocity of propagation (see Fig. 2 A, B) for both values of $K_{mns(Ca)}$ when ring is shortening to 16.364 cm (1024 nodes). These irregularities are more pronounced in the case of $K_{mns(Ca)} = 0.9$ mM, where the sensitivity of membrane current $I_{ns(Ca)}$ to $[Ca^{2+}]_i$ is increased. Accumulation of $[Ca^{2+}]_i$ causes spontaneous release from SR and increase of APD. Only the APs preceded by spontaneous Ca^{2+} release are elongated. The irregularities in both cases appear after spontaneous release significantly develops. The increase of APD leads to increase of the propagated wave length and later causes alternance of APD and velocity of propagation (especially for $K_{mns(Ca)} = 0.9$ mM).

c. The bump on the tail of propagating pulse and EADs appearance in some cells in a ring

Further shortening the ring length causes a new phenomenon, the appearance of bumps on the tail of the propagating pulse.

In the case when $K_{mns(Ca)} = 1.2$ mM (see Fig.3), shortening the ring length to 584 nodes (9.344 cm) leads to a sharp increase in irregularities of propagation (compare Fig. 2 A and Fig. 3A). Irregularities that occur prior to the appearance of spontaneous release can be attributed to the transient period associated with catching the high pacing rhythm in such a short ring. The bumps occurring on the tail are illustrated in Fig. 3B. In some cases they may cause a breakup of the tail before disappearing. The bumps can also be observed for longer ring lengths, but are not so pronounced.

Plotting wave shape and distribution of $[Ca^{2+}]_i$ on the same graph in Fig. 3B shows that the bump on the tail is caused by non-uniform $[Ca^{2+}]_i$ distribution in space. In this figure, (i) shows the $[Ca^{2+}]_i$ distribution corresponding to propagation time when spontaneous release has not yet developed. In (ii), we demonstrate the increase of wave length due to $[Ca^{2+}]_i$ accumulation and the beginning of subsequent spontaneous release (see trace of I_{spon} in Fig. 3A at time 2.03 s). There also a small bump is observed on a tail accompanied by a bump in Ca^{2+} distribution in the same region of cells. In (iii), we see a more pronounced bump on the tail of propagated pulse with corresponding significant increase of $[Ca^{2+}]_i$ in the cells of bump location. The increased $[Ca^{2+}]_i$ in these cells causes their APD to be higher than their neighbors. That why for some time, they are kept at higher potential level then their neighbors, which repolarized faster, causing in some cases the breakup of the tail. After some time the bump disappears because the cells in that region have negative dV/dt and are thus in repolarization phase. The only region of positive dV/dt in the ring is the front of the wave (Fig.3 B (iii).and 3C)

In this ring length we also observe instances where the front of the wave comes close to the tail and propagation is expected to stop. These instances can be seen in the graph of the velocity of propagation (Fig. 3A), where it reaches approximately one-third of its original value. It is impossible to determine from the calculation of propagation velocity whether propagation stops momentarily and then restarts, because that calculation is the result of an average velocity along a few cells and not it instantaneous

value. Instead, we look at the sign of dV/dt along the wave to determine whether propagation has truly stopped. We see (Fig. 3C) that when the front of the wave comes close to the tail, there are still a few cells at the wave front that have positive dV/dt . Thus, the wave never actually stops in this case.

In the case when $K_{mns(Ca)} = 0.9$ mM (see Fig.4), shortening the ring length to 920 nodes (14.72 cm) leads to highly irregular propagation (see Fig. 4A) and bumps on the tail much larger than the bumps observed for $K_{mns(Ca)} = 1.2$ mM (compare Fig.3C and Fig. 4C). In contrast to the previous case, it is possible to find among the bumps on the tail some with cells having $dV/dt > 0$. Looking at the shape of the wave at different times (see Fig. 4C), we first see the appearance of such bump on the tail ($t = 4.04$ s). The region of the bump has positive dV/dt , which causes the bump to become larger. As the original wave front comes closer to the bump, it slows down and decreases in magnitude. The original wave then stops completely and all its cells enter repolarization phase, while the bump produces a new propagating wave front ($t = 4.16$ s). The new wave front forms a new wave, and the old wave continues repolarization ($t = 4.28$ s).

The AP pattern shown in Fig. 4A directly indicates EAD for one particular cell in the region of the bump with $dV/dt > 0$. EADs occur in adjacent cells in the same turn, and all have the same shape. EAD occurs in repolarization phase of an AP that has been elongated by spontaneous release of Ca^{2+} . As a result of the EADs, APD for those cells is about twice as long as the APD for surrounding cells (see Fig. 4A).

In order to discern EAD from normal propagation, we look at the membrane currents of a cell in which an EAD occurred (see Fig. 4B). At the time of the EAD, there is no significant local current (I_N), the current that usually causes propagation from one cell to the next. Sodium current (I_{Na}), which typically supports depolarization, is also absent. The L-type Ca^{2+} channel current ($I_{Ca,L}$), not shown in the figure, is smaller than in the case of propagation. These graphs support the idea that the EAD is caused by an imbalance of inward and outward currents during the repolarization phase of an AP.

To further explore the effect of EAD on wave propagation, a shorter ring of 9.6 cm (600 nodes) is examined for the case of $K_{mns,Ca} = 0.9$ mM (see Fig. 5). Many EADs occur in cells of different regions of the ring and the occurrence of EAD is non-uniformly distributed in space (see Fig. 5B). More over, the character of EADs patterns in different nodes (#285 and #540 in Fig5A) in the ring is differing significantly. Among them it is possible to observe both single and multiple EADs. Velocity of propagation is highly irregular, as different wave fronts are stopping and starting. Calculation of APD along the ring is discarded because the presence of many EADs makes a single APD difficult to define. For the cell at node 540, the graphs of $[Ca^{2+}]_i$ and I_{spont} are also presented in the same figure. I_{spont} appears earlier than in previous cases, because $[Ca^{2+}]_i$ accumulates more quickly at the higher pacing rate.

Non-uniform distribution of EAD in space causes the wave to take on many interesting shapes, including the appearance of two distinct wave fronts (see Fig.5C). Two distinct regions of EAD occurring at the same time cause these wave fronts. The wave fronts may appear and move in the same direction (i) or in the opposite direction (ii). The ring is not long enough to contain two propagating waves. Therefore, when moving in the same direction, one wave front is close to the tail of the other. After some time it will stop, leaving only one propagating wave. When moving in opposite directions, the wave

fronts annihilate each other. Propagation stops temporarily until a new region of EAD appears to cause a new wave front.

Discussion

In the presented study we used the idealized form of ring-shaped tissue: the one-dimensional closed loop consisting of single cells connected in longitudinal direction by AP diffusion. It is assumed that extracellular and gap junction resistances are negligibly small compared to intracellular resistance. These assumptions allow us to use a one-domain approach in model formulation and to represent the tissue as a continuum. The use of such a 1D closed loop tissue creates the opportunity to easily change the number of nodes in a ring, and thus the period of wave circulation, which defines the pacing rate of the cells in a ring. At the same time, this approach allows elimination of specific properties of border conditions and the effects of wave front curvature encountered when wave propagates in 2D tissue. Thus, we can focus on the pure effect of Ca^{2+} dynamics on wave propagation under the condition of high pacing rate of tissue cells.

In [10] a new phenomenon was found – the appearance of bumps on the tail of propagated pulse in a ring of short length, with subsequent breakup of the tail. The bumps expressed nonmonotonic distribution of gradient $d\text{APD}/dx$ along the pulse length. That was observed for two different cases: (1) a ring composed of cell models with Ca^{2+} dynamics; and (2) a ring composed of cell models without Ca^{2+} dynamics, but with steep APD restitution. In the first case, the bumps are caused by non-uniform distribution of $[\text{Ca}^{2+}]_i$ in space. In the second case the steep restitution is responsible for nonmonotonic distribution of APD in space.

The presented results show that, depending on the sensitivity of Ca^{2+} dependent membrane currents (particularly $K_{\text{mns}(\text{Ca})}$ for $\text{Ins}_{(\text{Ca})}$) and amplitude of $[\text{Ca}^{2+}]_i$, the cells related to the bump have prolonged APD and may either be in repolarized phase with $dV/dt < 0$, or express EAD with $dV/dt > 0$. EADs are encountered in bumps only for $K_{\text{mns}(\text{Ca})} = 0.9$ mM and lead to the appearance of many distinct regions of EAD occurring at the same time and causing multiple wave fronts. The wave fronts may appear and move in the same direction or in the opposite direction. The ring is not long enough to contain two propagating waves. Therefore, when moving in the same direction, one wave front is close to the tail of the other. After some time it will stop, leaving only one propagating wave. When moving in opposite directions, the wave fronts annihilate each other. Propagation stops temporarily until a new region of EAD appears to cause a new wave front.

These properties of EAD in 2D tissue lead to formation of the island of the tissue with retarding repolarization and regeneration of nonstationary spiral wave in the direct or backward directions [20].

As it is well known, the Ca^{2+} dynamics models belong to the class of phenomenological models, with many unknown quantitative details. The ability of the model to reproduce $[\text{Ca}^{2+}]_i$ accumulation and connected spontaneous Ca^{2+} release from SR play a crucial role in wave propagation phenomena when tissue cells are under conditions of high pacing rates. Even recently proposed complicated models as [21, 22], like that used in this paper, can reproduce these phenomena only qualitatively. Thus, our

results can be regarded as qualitative and must be verified in direct physiological experiments. In this context, it is of great interest to show that it is possible to reach the similar results (without amplification of the effect of Ca^{2+} dynamics) by replacing in cell model the Hodgkin –Huxley representation of K_r channel gate processes on Markovian one [23], for which is characteristic that the open probability of rapid K^+ channels are decreased as the cell pacing rate increases.

Conclusion

The computer simulation of wave propagation in a ring composed of cell models, which reproduce the accumulation and Ca^{2+} spontaneous release under high pacing rate, shows that:

1. There exists a sufficiently short ring length when bumps occur on the tail of propagated pulse. These bumps are the expression of non-uniform distribution of APD along the cells involved in pulse propagation. This nonuniformity is the result of the difference in the period of cell stimulation and the period of spontaneous Ca^{2+} release from the SR. The bumps appear even in the case when the steepness of APD restitution is smaller than one.

2. Depending on the sensitivity of Ca^{2+} dependent currents on $[\text{Ca}]_i$ (in our study using different values of $K_{\text{mns}(\text{Ca})}$) and its amplitude, the cells related to the bump may have $dV/dt < 0$ or $dV/dt > 0$. In the first case, after significant decrease of the propagation velocity, the propagated pulse regenerates due to local current introducing irregularity in pulse propagation. In the second case the EADs are observed.

3. The EADs appear due to the distortion of a cell's repolarization phase currents toward the direction of a prevailing inward current. This occurred only for $K_{\text{mns}(\text{Ca})} = 0.9\text{mM}$. The region with EAD may stop the pulse propagation temporarily but then facilitates the wave regeneration in the original direction and even produces two wave front propagated temporary in the opposite directions.

Acknowledgments

The study was supported in part by NIH grant P50 HL52319. Supercomputing resources were provided by National Energy Research Scientific Computing Center, Office of Energy Research of the US Department of Energy, under the contract #DEAC0376SF00098.

References

1. Karma, A., Levine, H., and Zou, X. Theory of pulse instabilities in electrophysiological models of excitable tissues. *Physica D* 73, 113-127 (1994).
2. Chialvo, D., Gilmour, R., and Jalife, J. Low dimensional chaos in cardiac tissue. *Nature*, 343, 653-657 (1990).
3. Ito, H., and Glass, L. Theory of reentrant excitation in a ring of cardiac tissue. *Physica D* 56, 84-106 (1992).
4. Frame, L., and Simpson, M. Oscillations of conduction, action potential duration, and refractoriness. *Circulation* 78(5), 1277-1287, (1988).

5. Fei, H., Yazmajian, D., Hanna, M., Frame, L. Termination of reentry by lidocaine in the tricuspid ring in vitro. *Circ. Res.* 80, 242-252, (1997).
6. Zykov, V. *Simulation of Wave Processes in Excitable Media*. Manchester Univ. Press, Manchester, (1987).
7. Courtemanche, M., Glass, L., and Keener, J. Instabilities of a propagating pulse in a ring of excitable media. *Phys. Rev. Lett.* 70(14), 2182-2185, (1993).
8. Courtemanche, M., Keener, J. and Glass, L. Delay equation representation of pulse circulation in a ring in excitable media. *SIAM J. Appl. Math.* 56(3), 119-142, (1996).
9. Kogan, B., Karplus, W., Karpoukhin, M., Roizen, I., Chudin, E., and Qu, Z. Action potential duration restitution and electrical excitation propagation in a ring of cardiac cells. *Comp. and Biomed. Res.* 30, 349-359 (1997).
10. Chudin, E., Kogan, B. Pulse Propagation in a Ring-Shaped Cardiac Tissue Model with Intracellular Ca^{2+} Dynamics (Computer simulation study). *Mathematics and Computers in Modern Science*. Ed. N. Mastorakis. World Scientific and Engineering Society Press (2000)
11. Bassani, J. W., Bassani, R. A., Bers, D. M. Twitch-dependent SR Ca accumulation and release in rabbit ventricular myocytes. *Am. J. Physiol.* 265:C533-40. (1993)
12. Priori, S. G., Corr, P. B. Mechanisms underlying early and delayed afterdepolarizations induced by catecholamines. *Am. J. Physiol.* 258:H 1796-805.(1990)
13. Chudin, E., Goldhaber, J., Garfinkel, A., Weiss J., Kogan, B. Intracellular Ca^{++} dynamics and the stability of ventricular tachycardia. *Biophys. J.* 77, 2930- 2941 (1999).
14. Luo, C. H., and Rudy, Y. A dynamic model of the cardiac ventricular action potential. I. Simulations of ionic currents and concentration changes. *Circ. Res.* 74: 1071-1096 (1994)
15. Strang, G. *SIAM J. Numerical Analysis.* 5, 506-612. (1969).
16. Chudin, E., Garfinkel, A., Weiss, J., Karplus, W., Kogan, B. Wave propagation in cardiac tissue and effects of intracellular calcium dynamics (computer simulation study). *Prog Biophys Mol Biol.*;69:225-36. (1998)
17. Kogan, B.Y., Karplus, W. J., Chudin, E. E. Heart fibrillation and parallel supercomputers. In: *Proceedings of International Conference on Information and Control*. St. Petersburg, Russia;:857-865. (1997)
18. Winfree, A. T. Heart muscle as a reaction-diffusion medium: roles of electrical potential diffusion, activation front curvature, and anisotropy. *Int. J. Bif. & Chaos*,7:487-526. (1997)
19. Chudin, E. Instability of Cardiac Excitation Wave Propagation and Intracellular Calcium Dynamics. Dissertation for PhD degree in Biomathematics, UCLA (1999)
20. Kogan, B., Lamp, S., Weiss, J. Role of Intracellular Ca^{2+} Dynamics in Supporting Spiral Wave Propagation. Modeling and Simulation. Eds. George A. Bekey , Boris Y. Kogan. Kluwer Academic Publishers, pp177-193. (2003)
21. Noble, D., Varghese, A., Kohl, P., Noble, P. Improved guinea-pig ventricular cell model incorporating a dyadic space, I_{Kr} and I_{Ks} , and length-and tension-dependent processes. *Can. J. Cardiol*, Vol 14 , No 1 , pp123-134. (1998)
22. Greenstein, J. L. and Winslow, R. L. An Integrative model of the Cardiac Ventricular Myocyte Incorporating Local Control of Ca^{2+} Release. *Biophys J.* Vol . 83, pp2918-2945. (2002)
23. Kogan, B., Better, J., Zlochistyy, I. The cardiac cell model at normal and high pacing rates with Markovian representations of gating processes. Simulation in Biomedicine V. Eds. Z. M. Arnez, C.A. Brebbia, F. Solina, V. Stankovski. *WIT Press*, pp 15-24. (2003)

Appendix

a. Insufficient ring length

There exist ring lengths too short to sustain wave propagation. In these cases, upon closing of the ring the front of the wave immediately runs into its tail (see Fig. 6 B). The tail is still in repolarization phase, so the wave can no longer propagate in that direction. All nodes enter repolarization phase and eventually return to rest potential. The wave only makes one turn of the ring before stopping, and each node undergoes only one action potential. In the case of $K_{\text{mns}(\text{Ca})} = 1.2 \text{ mM}$, any ring equal to or shorter in length than 9.312 cm (582 nodes) will not allow for propagation (see Fig. 6 A). In the case of $K_{\text{mns}(\text{Ca})} = 0.9 \text{ mM}$, the critical length where propagation becomes no longer possible is 9.568 cm (598 nodes). Decreasing $K_{\text{mns}(\text{Ca})}$ has a small effect on the initial length of the wave, which is enough to prevent a wave from propagating in a ring that is suitable for propagation with normal $K_{\text{mns}(\text{Ca})}$.

b. Decrease of either \bar{G}_{kr} or \bar{G}_{ks}

\bar{G}_{kr} and \bar{G}_{ks} were decreased individually in an attempt to reproduce the phenomena that resulted from decreasing the value of $K_{\text{mns}(\text{Ca})}$. Decreasing \bar{G}_{kr} by approximately 50%, from 0.02614 mS/cm^2 to 0.01114 mS/cm^2 causes the appearance of EAD even under normal sensitivity to Ca^{2+} (see Fig. 7 A). Unlike the case of decreased $K_{\text{mns}(\text{Ca})}$, however, these EADs do not maintain wave propagation by starting a new propagating wavefront. Instead, the region of EAD causes the old wavefront to stop and all nodes enter repolarization phase. Propagation never restarts since a new wavefront does not appear. Decreasing \bar{G}_{kr} further, to 0.005 mS/cm^2 , causes the appearance of multiple EADs (see Fig. 7 B). These EADs do not cause new wavefronts to appear either. The inability of the EADs to create new wavefronts prevents the appearance of multiple wavefronts at the same time, moving in the same or opposite directions. Thus, simply decreasing \bar{G}_{kr} does not give the same effect as decreasing $K_{\text{mns}(\text{Ca})}$ did.

Decreasing \bar{G}_{ks} from its standard value of 0.28 mS/cm^2 has the same effect as did decreasing \bar{G}_{kr} . Decreases of about 50% (to 0.117 mS/cm^2) yield EADs and larger decreases (to 0.07 mS/cm^2) yield multiple EADs. However, these EADs cannot cause the appearance of new wavefronts.

c. Decrease of $K_{\text{mns}(\text{Ca})}$ and either \bar{G}_{kr} or \bar{G}_{ks}

Decreasing $K_{\text{mns}(\text{Ca})}$ in conjunction with a decrease in either \bar{G}_{kr} or \bar{G}_{ks} leads to new results. For the ring length where decreasing \bar{G}_{kr} alone leads to single EADs (11.264 cm, 704 nodes), when $K_{\text{mns}(\text{Ca})}$ is decreased to 1.0 mM the simulation results in multiple EADs (see Fig. 8 A). As before, however, these EADs do not cause new wavefronts to

appear. Decreasing $K_{\text{mns}(\text{Ca})}$ further to 0.9 mM for the same ring length and value of \overline{G}_{kr} causes the appearance of a non-rest equilibrium state (see Fig 8 B). The nodes undergo multiple EADs of decreasing magnitude, until settling into an equilibrium value of -16 mV. All nodes of the ring reach the same equilibrium value.

The same results hold for decreasing $K_{\text{mns}(\text{Ca})}$ and \overline{G}_{ks} . While a \overline{G}_{ks} value of 0.117 mS/cm² and a ring length of 13.312 cm (832 nodes) causes a single EAD, when $K_{\text{mns}(\text{Ca})}$ is decreased to 1.1 mM we see instead multiple EADs. Decreasing $K_{\text{mns}(\text{Ca})}$ further, to 1.0 mM, leads to the appearance of a non-rest equilibrium state.

d. Increase of $I_{p(\text{Ca})}$ in conjunction with decrease of either \overline{G}_{kr} or \overline{G}_{ks}

Increasing the $I_{p(\text{Ca})}$ current while also decreasing either \overline{G}_{kr} or \overline{G}_{ks} has the same effect as decreasing $K_{\text{mns}(\text{Ca})}$ while also decreasing either \overline{G}_{kr} or \overline{G}_{ks} . Lengths of the ring (11.264 cm) and \overline{G}_{kr} values (0.01114 mS/cm²) that led to single EADs before now result in multiple EADs when $I_{p(\text{Ca})}$ is increased to 135% its normal value. As with the other experiments with decreasing \overline{G}_{kr} and \overline{G}_{ks} , though, the EADs still do not cause new wavefronts. Increasing $I_{p(\text{Ca})}$ to 150% its normal value causes the appearance of a non-rest equilibrium state. The equilibrium state is slightly different (-15 mV) than the state resulting from decreased $K_{\text{mns}(\text{Ca})}$. Increasing the value of $I_{p(\text{Ca})}$ by the same amounts while keeping \overline{G}_{ks} at 0.117 mS/cm² and the ring length at 13.312 cm yields the same results.

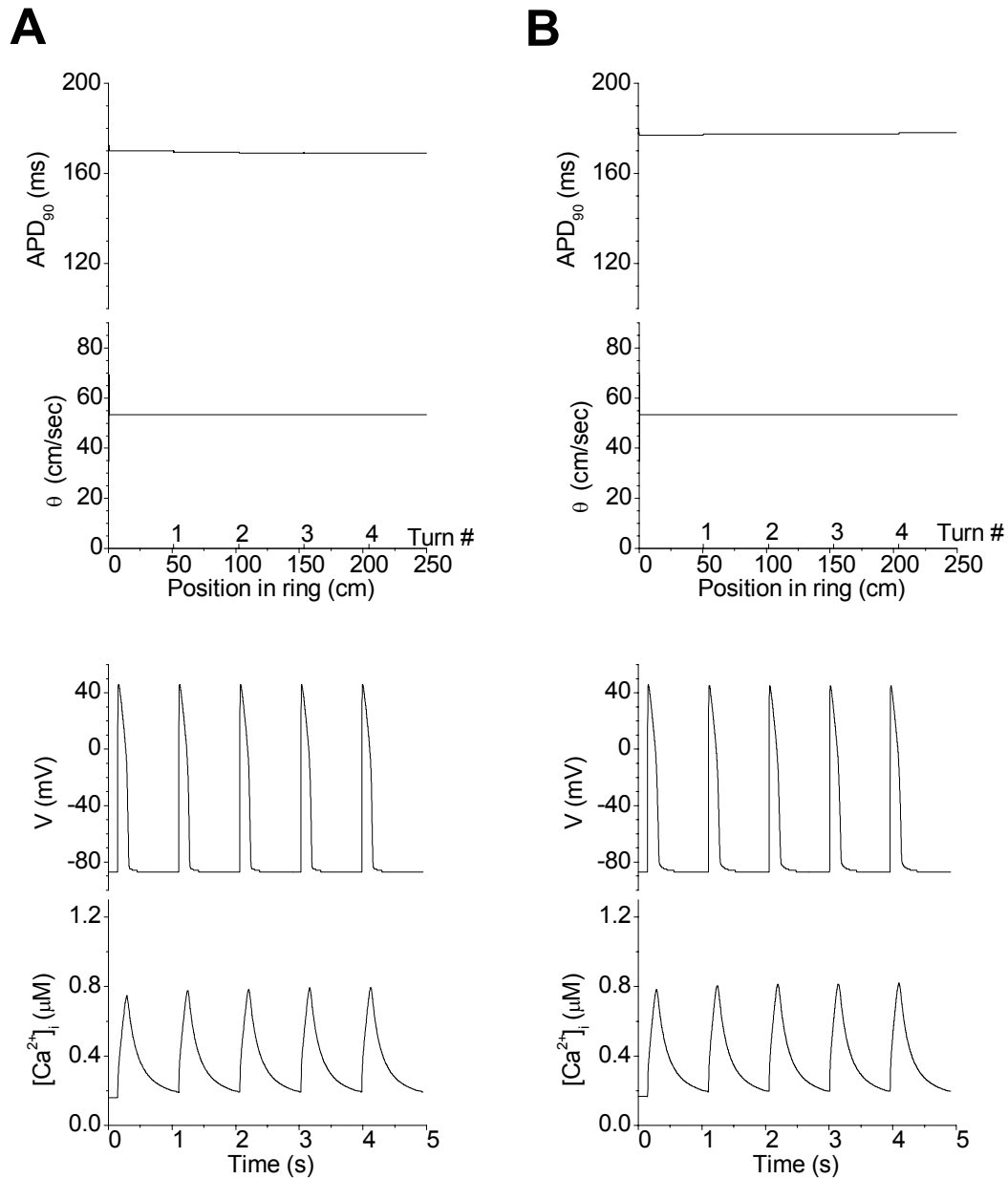


Fig 1. Stationary propagation

Ring Length = 51.2 cm (3200 nodes), $T = 960 \text{ ms}$

A: $K_{mns(Ca)} = 1.2 \text{ mM}$

B: $K_{mns(Ca)} = 0.9 \text{ mM}$

V and $[Ca^{2+}]_i$ measured in node 500. No I_{spon} was observed.

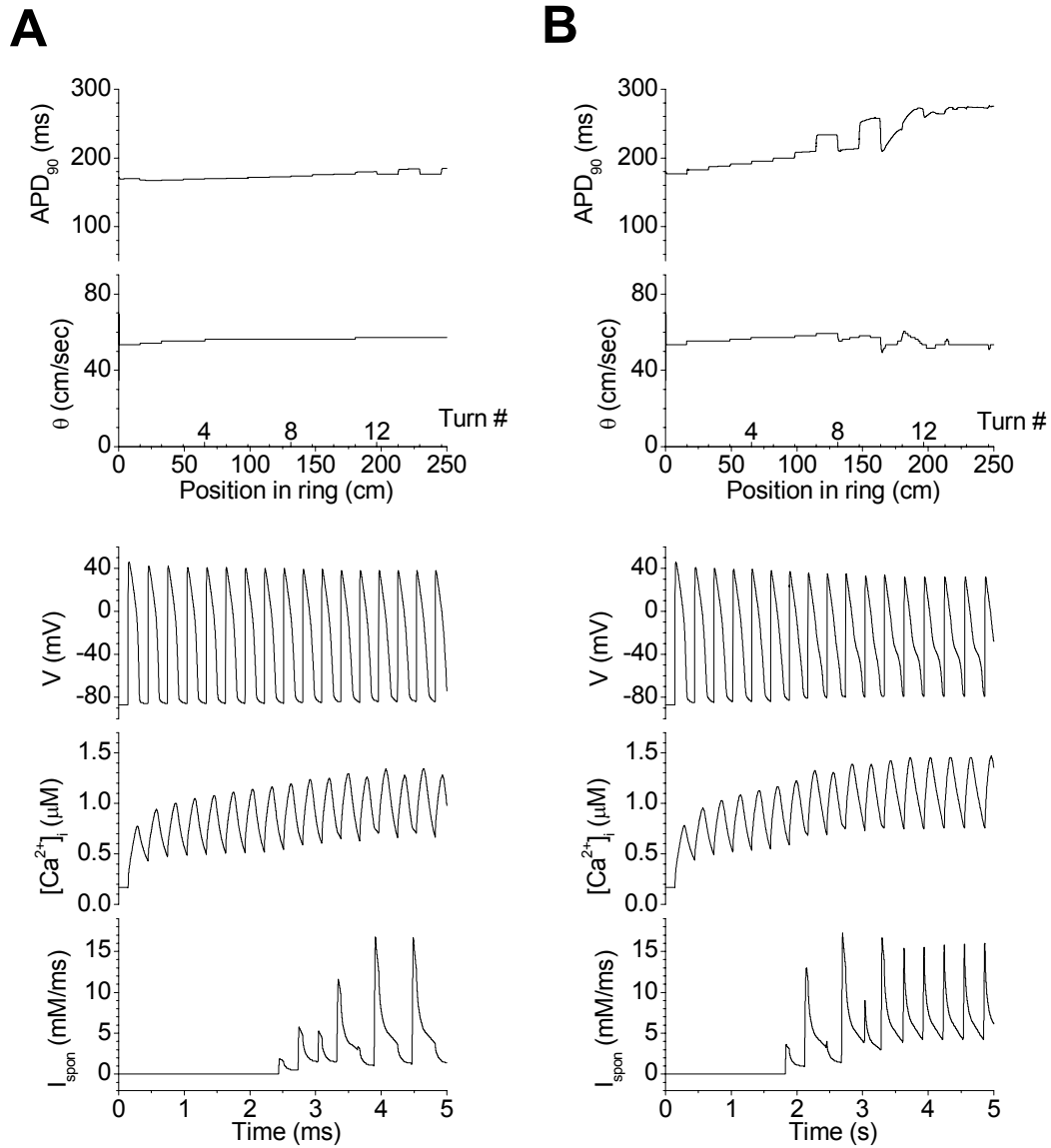


Fig 2. **Beginning of nonstationary propagation**
 Ring Length = 16.384 cm (1024 nodes), $T = 295$ ms

A: $K_{mns(Ca)} = 1.2$ mM

B: $K_{mns(Ca)} = 0.9$ mM

V , $[Ca^{2+}]_i$, and I_{spont} measured in node 500.

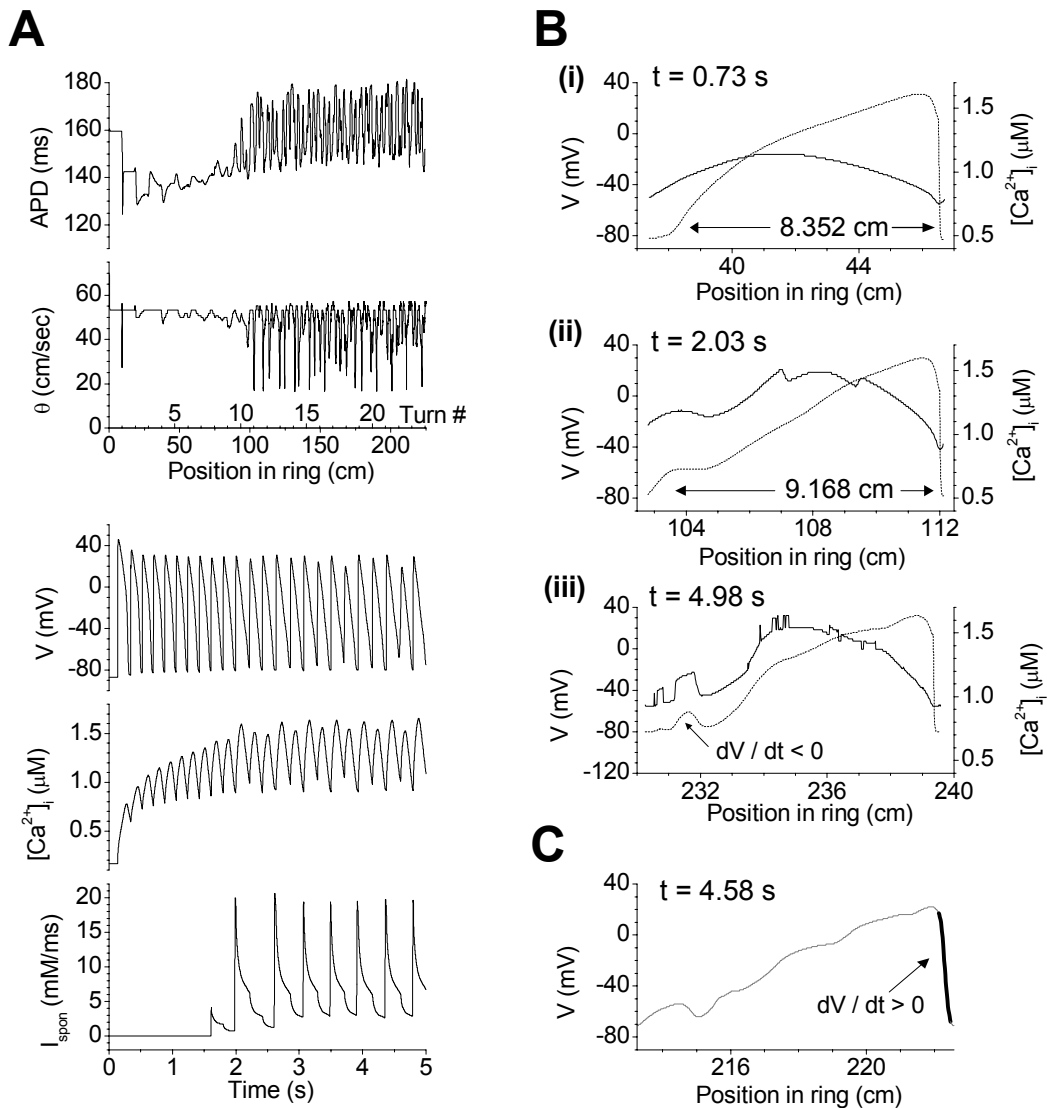


Fig 3. Irregular propagation

$K_{mns(Ca)} = 1.2$ mM, Ring Length = 9.344 cm (584 nodes), $T = 194$ ms

A: Major characteristics of wave propagation. APD calculated using threshold of -50 mV. V , $[Ca^{2+}]_i$, and I_{spon} measured in node 500.

B: Shape of wave (dotted line) and distribution of $[Ca^{2+}]_i$ in space (solid line) at different moments in time. In (i) and (ii), the length of the wave is shown. In (iii), the region of the bump on the tail of the wave is shown to have negative dV/dt .

C: Shape of the wave in the case of the wave front coming very close to the tail. The front of the wave has positive dV/dt , though smaller than found in a normal propagating wave front (where $dV/dt > 10$).

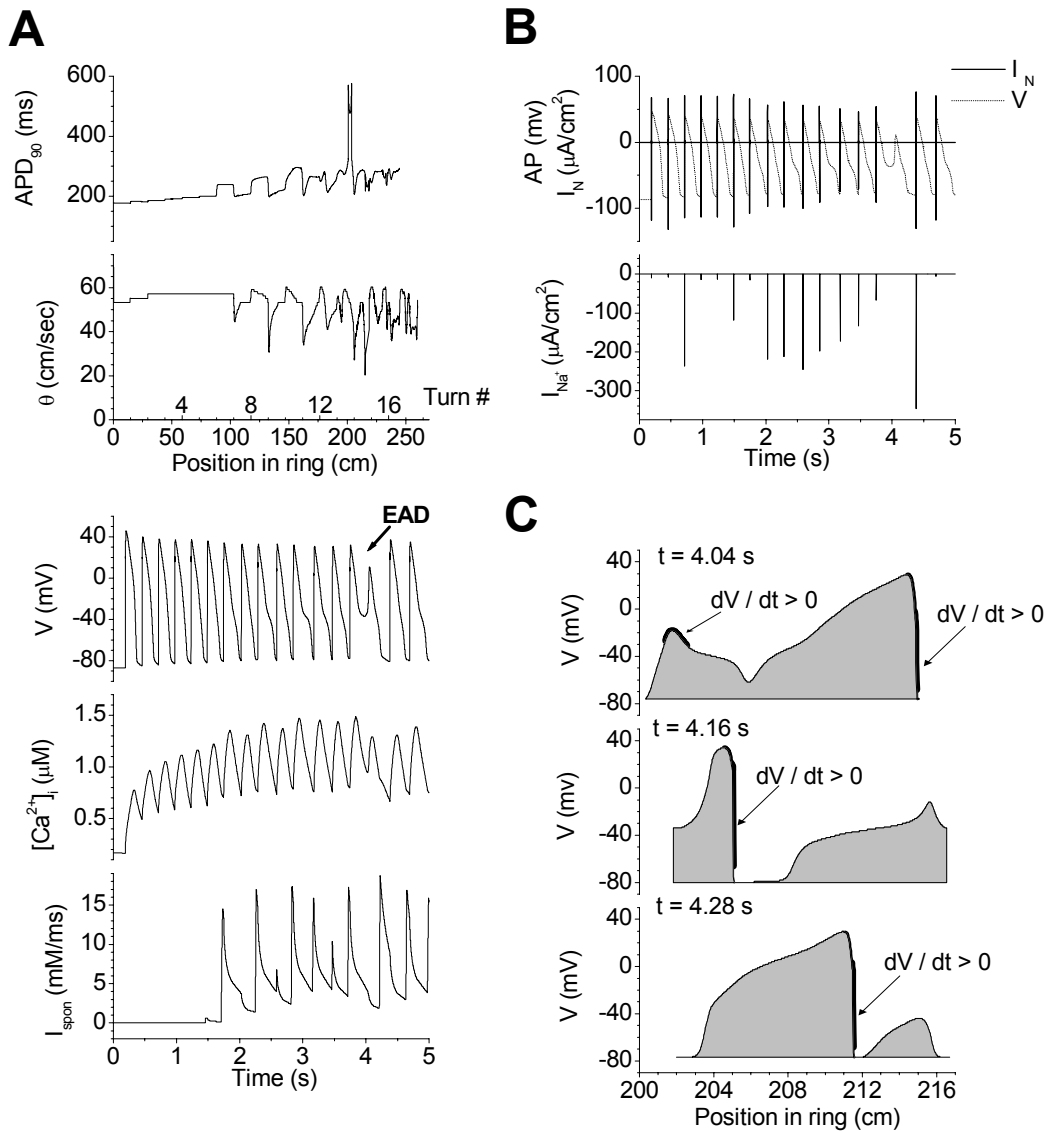


Fig 4. Appearance of EAD

$K_{mns(Ca)} = 0.9$ mM, Ring Length = 14.72 cm (920 nodes), $T = 265$ ms

A: Major characteristics of wave propagation. V , $[Ca^{2+}]_i$, and I_{spon} measured in node 653. EAD pointed out in graph of V .

B: Certain membrane currents for node 653, a node where EAD occurred.

C: Shape of the wave at different moments in time during wave regeneration by regions of EAD. Regions of positive dV/dt are darkened and pointed out.

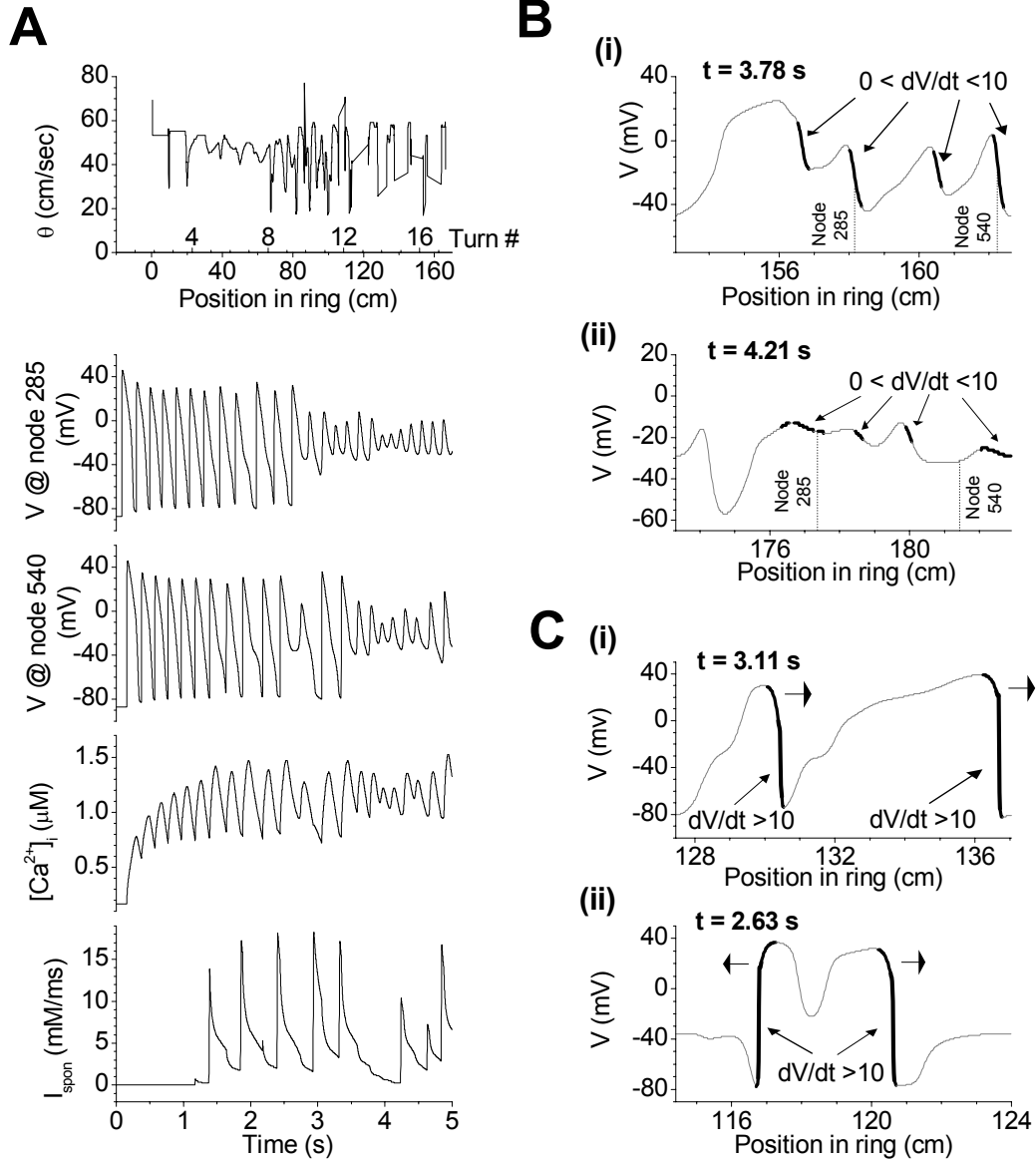


Fig 5. Effect of many EADs

$K_{mns(Ca)} = 0.9$ mM, Ring Length = 9.6 cm (600 nodes), $T = 185$ ms

A: Major characteristics of wave propagation. V measured in node 285 and node 540. $[Ca^{2+}]_i$, and I_{spn} measured in node 540.

B: Shape of wave at moments in time where many regions of EAD exist. Regions of positive dV/dt are darkened and pointed out. Regions of $dV/dt > 10$ represent a propagating wave front, while regions of $0 < dV/dt < 10$ represent regions of EAD. Dotted vertical lines show the positions of node 285 and node 540.

C: Shape of wave at different moments in time where two propagating wave fronts occur. Curve is darkened in regions of positive dV/dt . Regions of $dV/dt > 10$, indicating a propagating wave front, are pointed out.

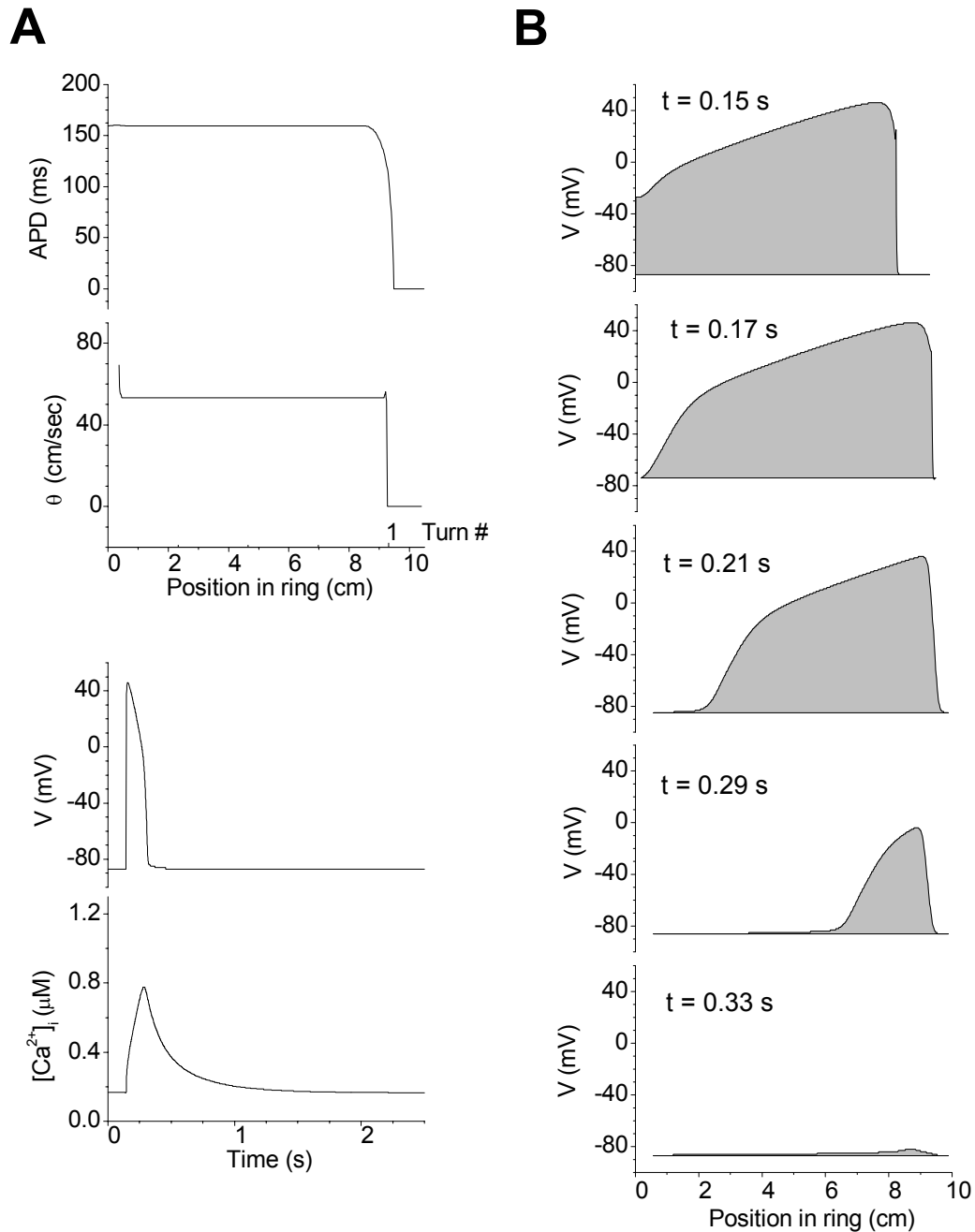


Fig 6. Wave termination due to insufficient ring length

Ring Length = 9.312 cm (582 nodes), $K_{mns(Ca)} = 1.2$ mM

A: Major characteristics of wave propagation. APD calculated using threshold of -50 mV. V and $[Ca^{2+}]_i$ measured in node 500. No I_{spon} was observed.

B: Shape of the wave at different moments in time.

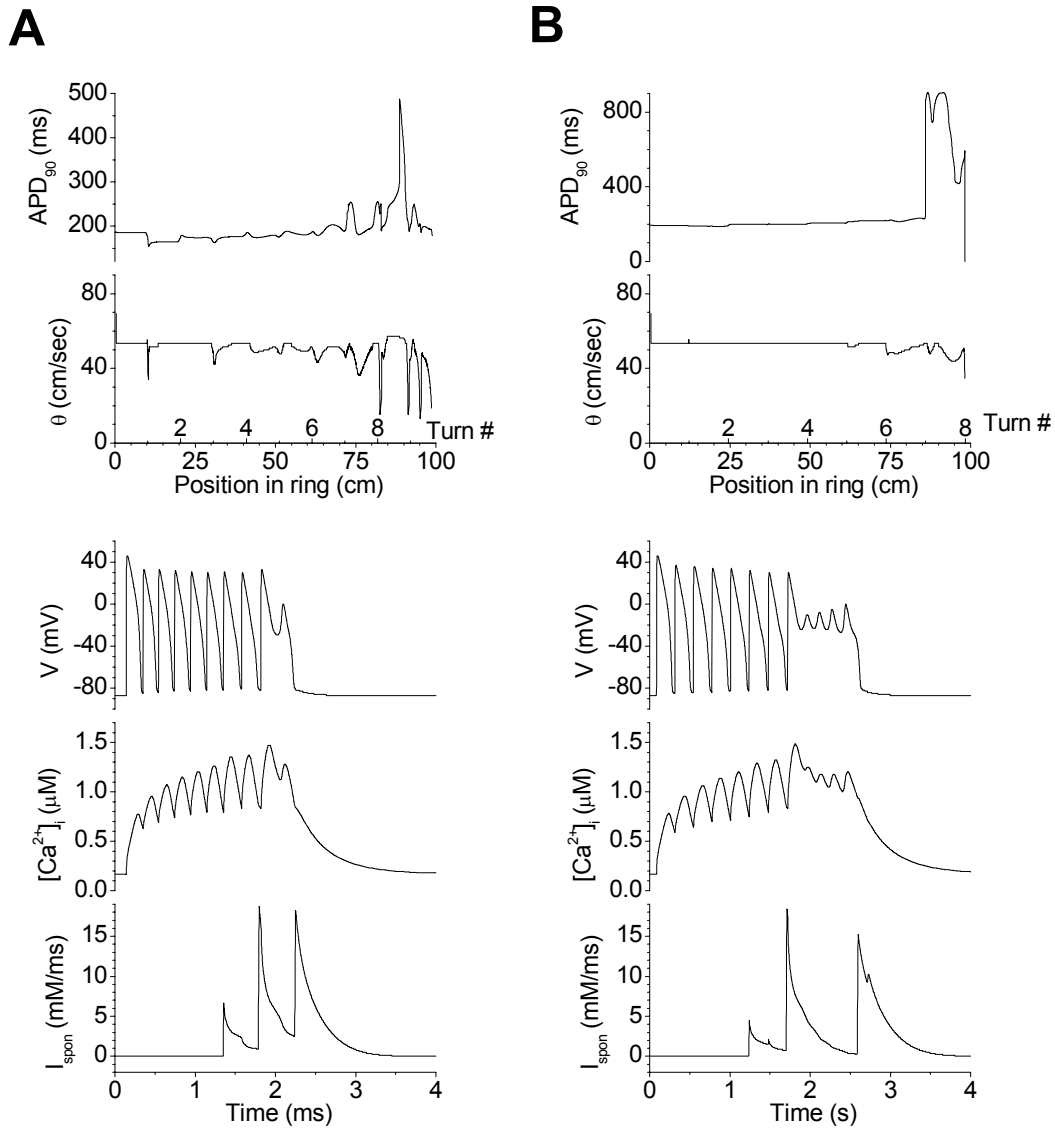


Fig 7. **Decreased \bar{G}_{kr}**

A: $\bar{G}_{kr} = 0.01114$ mS/cm², Ring Length = 10.112 cm (632 nodes). V , $[Ca^{2+}]_i$, and I_{spon} measured in node 487.

B: $\bar{G}_{kr} = 0.005$ mS/cm², Ring Length = 12.288 cm (768 nodes). V , $[Ca^{2+}]_i$, and I_{spon} measured in node 300.

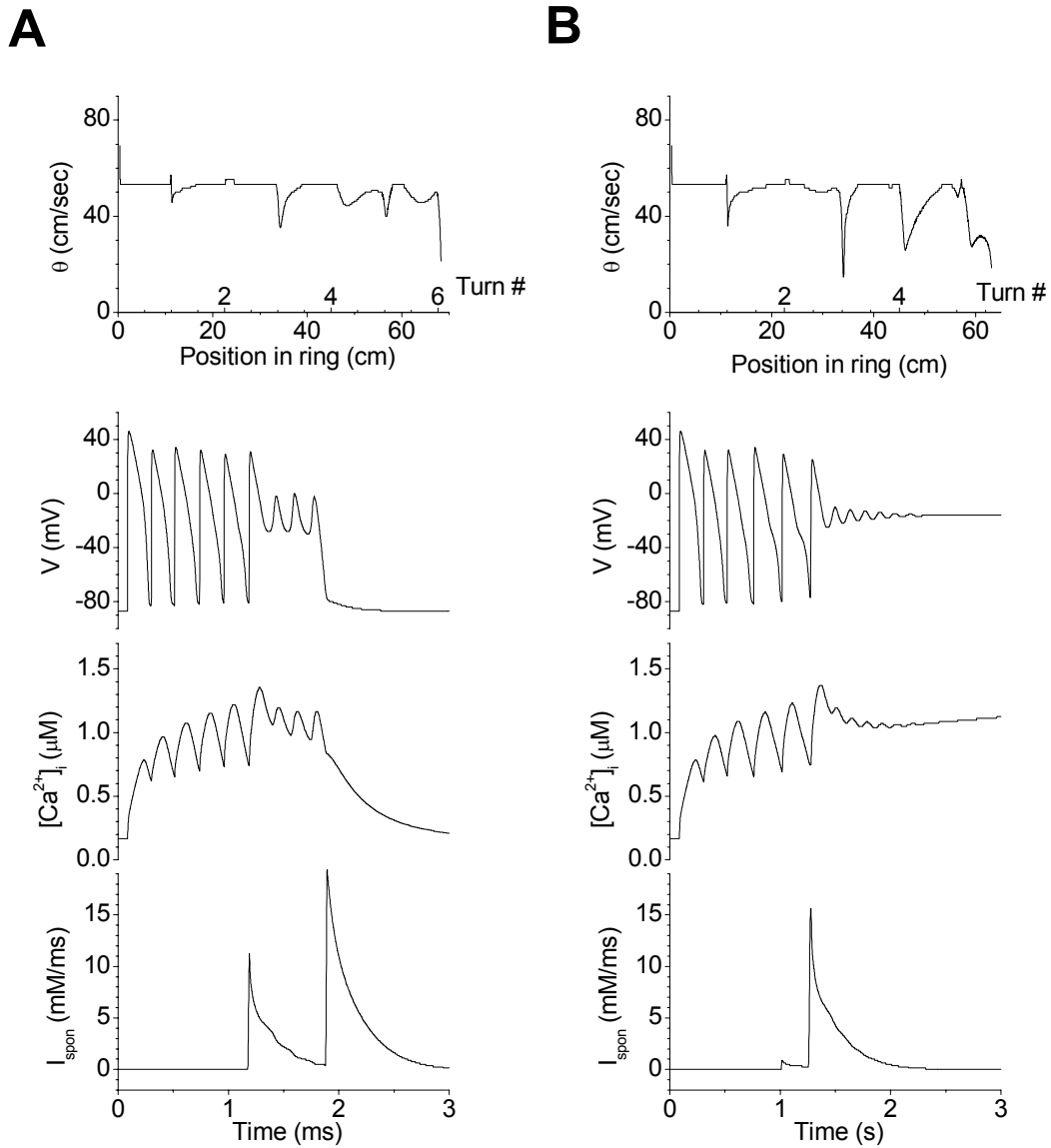


Fig 8. **Decreased \bar{G}_{kr} and decreased $K_{\text{mns(Ca)}}$**

$\bar{G}_{kr} = 0.01114 \text{ mS/cm}^2$, Ring Length = 11.264 cm (704 nodes). V , $[\text{Ca}^{2+}]_i$, and I_{spon} measured in node 300.

A: $K_{\text{mns(Ca)}} = 1.0 \text{ mM}$

B: $K_{\text{mns(Ca)}} = 0.9 \text{ mM}$

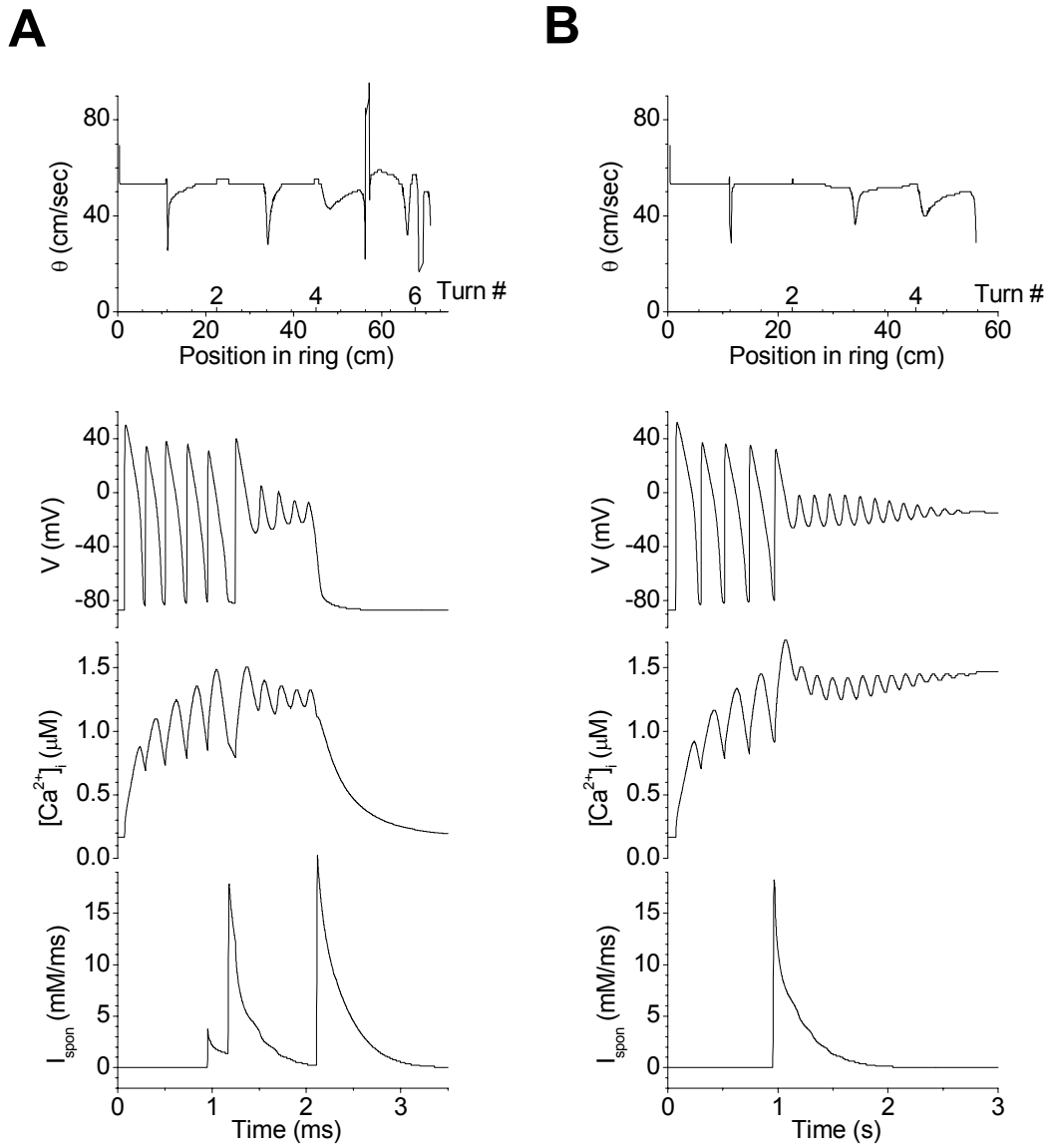


Fig 9. **Decreased \bar{G}_{kr} and increased $I_{\text{p(ca)}}$**

$\bar{G}_{kr} = 0.01114 \text{ mS/cm}^2$, Ring Length = 11.264 cm (704 nodes). V , $[\text{Ca}^{2+}]_i$, and I_{spon} measured in node 259.

A: 135% $I_{\text{p(ca)}}$

B: 150% $I_{\text{p(ca)}}$